THE JOURNAL OF PHYSICAL CHEMISTRY B

Article

pubs.acs.org/JPCB

Origins of Structural Flexibility in Protein-Based Supramolecular Polymers Revealed by DEER Spectroscopy

Nathan A. Tavenor,[†] K. Ishara Silva,[†] Sunil Saxena,* and W. Seth Horne*

Department of Chemistry, University of Pittsburgh, Pittsburgh, Pennsylvania 15260, United States

Supporting Information

ABSTRACT: Modular assembly of bio-inspired supramolecular polymers is a powerful technique to develop new soft nanomaterials, and protein folding is a versatile basis for preparing such materials. Previous work demonstrated a significant difference in the physical properties of closely related supramolecular polymers composed of building blocks in which identical coiled-coil-forming peptides are cross-linked by one of two subtly different organic linkers (one flexible and the other rigid). Herein, we investigate the molecular basis for this observation by isolating a single subunit of the supramolecular polymer chain and probing its structure and conformational flexibility by double electron−electron resonance (DEER) spectroscopy. Experimental spin−spin distance distributions for two different labeling sites coupled with molecular dynamics simulations provide insights into how the linker structure impacts chain dynamics in the coiled-coil supramolecular polymer.

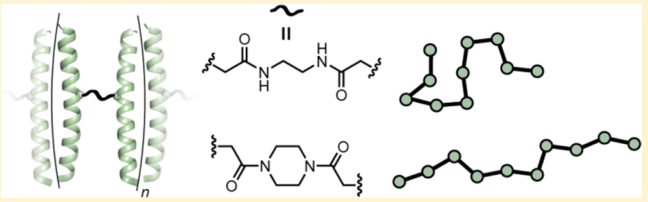

INTRODUCTION

Supramolecular polymers are a class of materials characterized by their polymerization through noncovalent interactions (hydrogen bonding, metal chelation, hydrophobic interactions, etc.) as opposed to classical polymers that are connected through covalent bonds.[1−3] Compared to classical polymers, supramolecular polymers can be more readily disassembled by external stimuli,[2,4] leading to their use in the design of environmentally responsive "smart" materials for various applications including analytical devices, regenerative medicine, and organic electronics.[4−8] Understanding the fundamental relationship between chain dynamics and macroscopic properties of supramolecular polymer materials is essential to their ongoing use in such applications.

One promising approach to the construction of supramolecular materials involves the use of protein−protein binding interactions as the noncovalent forces that drive assembly.[9,10] In such work, the α-helical coiled-coil folding motif has shown itself to be particularly valuable. The coiled coil is a protein quaternary structure made up of short α-helical peptides that assemble into supramolecular bundles.[11] The sequences that give rise to these assemblies can be designed with fine control over oligomerization state, stability, and topology of the folded structure.[12−16] Prior work has shown that supramolecular polymers can be prepared from appropriately designed subunits containing coiled-coil-forming peptides. Both hollow[17] and solid nanofibers[9] have been prepared using building blocks that are either strictly peptidic[18,19] or made up of multiple chains connected by an organic linker.[20,21]

We have recently reported an approach to coiled-coil supramolecular polymers based on the programmed self-assembly of subunits composed of two ∼4 kDa coiled-coil-forming peptides linked at their midpoints by a simple organic linker (Figure 1).[21,22] The linker, based on either an ethylenediamide (EDA) or piperazine (PIP) core, connects

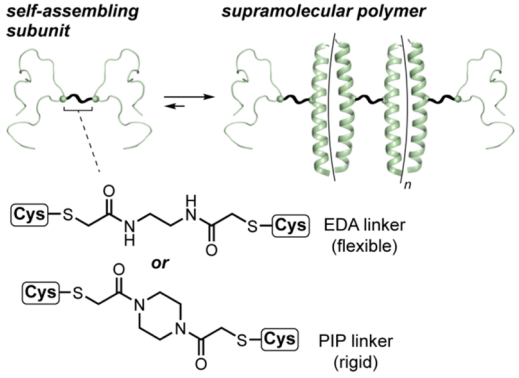

Figure 1. A subunit building block consisting of two α-helical coiled-coil-forming peptide sequences can spontaneously self-assemble to form a supramolecular polymer. The structure of the organic linker that connects the chains has a significant effect on assembly properties.

the two peptide domains via solvent-exposed Cys residues. The EDA and PIP linkers separate the peptide chains by the same number of atoms, but they differ in rigidity (EDA has three additional freely rotatable bonds compared to PIP). Despite the close structural similarity of subunits based on these two linkers (only two added CH_2 groups in a 8 kDa macromolecule), the supramolecular materials formed by each showed very different physical properties. Specifically, a subunit based on the PIP

Received: June 6, 2014
Revised: July 24, 2014
Published: July 24, 2014

   dx.doi.org/10.1021/jp505643w | J. Phys. Chem. B 2014, 118, 9881−9889

linker gave rise to assemblies with a larger apparent hydrodynamic diameter than a related subunit with the same peptide domains appended to EDA.[21] These results suggest that linker rigidity is an essential parameter for controlling supramolecular polymer structure.

An unanswered question in the above-described work is the physical basis for the different impact of the PIP and EDA linker structure on the formation of coiled-coil supramolecular polymers. From first principles, the PIP linker would be expected to give rise to stiffer supramolecular chains; however, this hypothesis is difficult to test directly. Underlying this challenge is the need to obtain precise measurements of the conformational distributions of the cross-linked subunits in the context of a supramolecular assembly. In an effort to probe these characteristics in greater detail, we utilized DEER spectroscopy, a type of pulsed electron spin resonance (ESR) spectroscopy that allows interspin distances to be measured. The DEER method is capable of measuring distance distributions in the range of 1.5−10 nm,[23−26] making it potentially well suited to probe the structure in protein-based supramolecular polymers.

EXPERIMENTAL SECTION

Synthesis of Peptides 1−5 and 10−12. Peptides were prepared by Fmoc solid-phase peptide synthesis[27] manually using a MARS microwave reactor (CEM), in automated fashion on a Tribute synthesizer (Protein Technologies), or a combination of both. NovaPEG Rink Amide resin was used as the solid support. Standard automated couplings were carried out with 5 equiv of Fmoc amino acid and 4.9 equiv of 2-(6-chloro-1*H*-benzotriazole-1-yl)-1,1,3,3,-tetramethyluronium hexafluorophosphate (HCTU) in a solvent of 4.4% *N*-methylmorpholine in *N*,*N*-dimethylformamide (DMF). Standard microwave couplings were carried out with 5 equiv of Fmoc amino acid, 4.9 equiv of HCTU, and 7.5 equiv of diisopropylethylamine (DIEA) in *N*-methyl-2-pyrrolidinone. A solution of 20% 4-methylpiperidine in DMF was used for Fmoc deprotection.

Fmoc-Ahx-OH was incorporated using the standard automated protocol with benzotriazol-1-yl-oxytripyrrolidinophosphonium hexafluorophosphate (PyBOP) in place of HCTU, and the next two residues were double-coupled. TOAC was incorporated as the free amino acid using the standard microwave protocol but with PyBOP in place of HCTU and double the reaction time. The residue following TOAC was activated as the acid fluoride[28] and subjected to 2−3 coupling reactions for extended times using microwave coupling conditions to ensure complete acylation of the highly hindered N-terminal amine. Acetylation of the peptide N-terminus was carried out on resin by treatment with 8:2:1 by volume DMF/DIEA/Ac_2O. N-terminal modification with 4-acetamidobenzoic acid was carried out on resin using standard microwave coupling conditions but with bromotripyrrolidinophosphonium hexafluorophosphate (PyBrOP) in place of HCTU.

Peptides were cleaved from resin using a solution of trifluoroacetic acid (TFA) and scavengers for 3−6 h. Scavenger cocktails were as follows (all ratios by volume): TFA/H_2O/ethanedithiol (EDT)/triisopropylsilane (TIS) in a ratio of 92:3:3:1 for peptides **1**, **2**, and **4**; TFA/H_2O/anisole/TIS in a ratio of 91:3:3:3 for peptide **5**; TFA/H_2O/EDT/anisole/TIS in a ratio of 90:3:3:3:1 for peptide **10**; and TFA/H_2O/TIS/anisole in a ratio of 85:5:5:5 for peptides **11** and **12**. Thiol scavengers were omitted in cleavage of nitroxide-containing peptides to avoid an irreversible side reaction.[29]

Crude peptides were precipitated by addition of ice-cold ether, centrifuged into a pellet, and purified by preparative reverse-phase HPLC on a C18 column (Phenomenex) using gradients between water and acetonitrile with 0.1% TFA. For peptides containing nitroxides, 10% (v/v) aqueous ammonium hydroxide was added to regenerate the radical prior to HPLC purification.[29,30] Peptides **11** and **12** were further purified by ion exchange chromatography on a Mono Q 5/50 GL column (GE Healthcare) using a gradient between 20 mM ammonium formate, pH 7.7 and 0.5 M ammonium formate, pH 7.7. Peptide **3** was prepared by reaction of the Cys residue in purified peptide **2** with (1-oxyl-2,2,5,5-tetramethylpyrroline-3-methyl)methanethiosulfonate (MTSSL). A 50 μM solution of peptide **2** was prepared in 50 mM phosphate, 300 mM NaCl, pH 6.55; the solution was cooled on ice, and MTSSL was added to a final concentration of 500 μM. After 20 min, the mixture was purified by preparative HPLC. The identity and purity of the final products were confirmed by MALDI-MS and analytical HPLC, respectively. Peptide stock concentrations were determined by UV−vis spectroscopy using the extinction coefficients listed in Table S1, Supporting Information.

X-ray Crystallography. Peptide **4** was crystallized by hanging drop vapor diffusion. A stock solution of peptide in water (10 mg/mL) was mixed (0.7 μL + 0.7 μL) with a crystallization buffer composed of 0.2 M sodium citrate tribasic, 0.1 M sodium cacodylate (pH 6.5), and 30% (v/v) isopropanol and allowed to equilibrate at room temperature over a well of 0.7 mL of crystallization buffer. A single crystal of **4** was flash frozen in liquid nitrogen after cryoprotection in a well buffer containing 30% (v/v) glycerol. Diffraction data were collected using Cu K_α radiation on a Rigaku/MSC diffractometer (FR-E generator, VariMax optics, Raxis HTC image plate detector) equipped with an X-Stream 2000 low-temperature system operated at 100 K. Raw diffraction data were processed with d*TREK. The structure was solved by molecular replacement using a published structure of the dimer formed by peptide **1** (PDB 4DMD) as a search model. Refinement was carried out using the Phenix software suite[31] and manual model building performed with Coot.[32] Data collection and refinement statistics are given in Table S2, Supporting Information.

Synthesis of Linker 7. To a stirred solution of PIP (421 mg, 4.9 mmol, 1 equiv) in 4 mL of chloroform at 0 °C were simultaneously added via addition funnels 1.05 mL of iodoacetyl chloride (14.7 mmol, 3 equiv) in 5 mL of chloroform and 1.68 g of K_2CO_3 (12.25 mmol, 2.5 equiv) in 5 mL of water. The solution was allowed to warm to room temperature and stirred 2 h. The organic layer was isolated by extraction, concentrated, and purified using column chromatography (50% ethyl acetate in acetone). Fractions containing the product were concentrated, redissolved in chloroform, and filtered. The filtrate was concentrated and dried under vacuum to afford the product as a pale yellow solid (0.451 g, 1.07 mmol, 22% yield). ^{1}H NMR (400 MHz, DMSO-d_6): δ 3.92 (d, J = 11.6 Hz, 4H), 3.47 (m, 8H). ^{13}C NMR (100 MHz, DMSO-d_6): δ 166.7, 166.5, 46.0, 45.8, 41.2, 41.1, −1.2, and −1.4. HRMS m/z calculated for $C_8H_{12}I_2N_2O_2$ $[M + H]^+$: 422.9067; found 422.9078.

Synthesis of Subunits 8, 9, 13, and 14. A fresh 2 mM stock solution of linker **6** (synthesized as previously described[21]) or linker **7** was prepared in DMF. Cys-functionalized peptide (**2** or **10**) was dissolved at 100 μM concentration

in 25 mM phosphate buffer at pH 7 and heated to 60−70 °C. An aliquot of linker (0.1 equiv) was added every 15 min until five aliquots had been added, for a final linker concentration of 50 μM. After addition of the final aliquot, the reaction was allowed to continue for another hour and then quenched by addition of 1:1 water/acetonitrile with 0.1% TFA. The solution was concentrated by centrifugation through a 3 kDa cutoff filter, diluted with ∼10 mL of water, and then recentrifuged to a final volume of ∼2 mL. Subunits were purified by preparative reverse-phase HPLC on a C18 column using gradients between water and acetonitrile with 0.1% (**8** and **9**) or 1% TFA (**13** and **14**). The identity and purity of the final products were confirmed by MALDI-MS and analytical HPLC, respectively. Subunit stock concentrations were determined by UV−vis spectroscopy using the extinction coefficients listed in Table S1, Supporting Information.

Double Electron−Electron Resonance (DEER) Spectroscopy. DEER experiments were performed on either a Bruker ElexSys E580 or a Bruker ElexSys E680 X-band FT/CW spectrometer equipped with a Bruker ER4118-MD5 or EN4118X-MD4 resonator, respectively. The sample temperature was regulated using an Oxford ITC503 temperature controller and an Oxford CLT650 low-loss transfer tube. For each measurement, ∼150 μL of the appropriate sample was transferred into a 3 mm inner diameter quartz tube, flash frozen in liquefied methylacetylene-propadiene and propane (MAPP) gas, and inserted into a sample cavity precooled to 80 K. The four-pulse DEER experiments were carried out using a pulse sequence of $(\pi/2)\nu_1$-τ_1-$(\pi)\nu_1$-T-$(\pi)\nu_2$-τ_2-$(\pi)\nu_1$-τ_2-echo.[33] The pump frequency ν_2 was set at the maximum of the nitroxide spectrum. The observer frequency ν_1 was offset by ∼70 MHz. The lengths of the $(\pi/2)\nu_1$ and $(\pi)\nu_1$ pulses were 16 and 32 ns, respectively. The $(\pi)\nu_2$ pulse was set to 16 ns. Step sizes of 8 and 16 ns were used to measure shorter and longer distances, respectively, for 128 data points. Deuterated solvent and glycerol-d_8 were used to increase the phase memory time of samples that were expected to give longer distances. Raw DEER data were analyzed using the DEERAnalysis2013[34] software. Given the scope of the present work, where general features of the distance distributions were needed, we analyzed the data assuming a Gaussian distance distribution. Although model-dependent, such fits improve the reliability of the analysis.[34] The use of Gaussian models also facilitates comparison of trends in closely related samples and minimizes artifacts arising from low signal-to-noise, which can complicate data interpretation.

Circular Dichroism (CD) Spectroscopy. CD measurements were performed in 1 mm quartz cuvettes on an Olis DSM 17 CD spectrometer. All buffer components were syringe-filtered through a 0.22 μm pore filter prior to use. Scans were acquired at 20 °C in the range of 200−260 nm with a 2 nm bandwidth, 1 nm increment, and 5 s integration time. Thermal melts were measured at 222 nm with a 2 nm bandwidth and a 2 min equilibration at each temperature. All samples were baseline-corrected with buffer blanks measured in the same cuvette. Thermal melts were fit to a two-state unfolding model using GraphPad Prism.

Molecular Dynamics (MD)-Aided Modeling of Capped Subunits. MD simulations were performed using the GROMACS 4.6.3 software package[35] and the AMBER99sb-ildn force field.[36] Amber-compatible force field parameters for the EDA and PIP linkers capped with thioethyl groups (EDA-Et_2 and PIP-Et_2) were prepared using Antechamber[37] and acpype.[38] Three separate simulations of the linkers were performed, one for EDA-Et_2, one for PIP-Et_2 with the two amide carbonyls pointing in the same direction (*cis*-PIP-Et_2), and one with the two amide carbonyls pointing in opposite directions (*trans*-PIP-Et_2). The two different starting conformers of PIP were run separately because tertiary amide isomerization is not effectively sampled on the time scale of the simulations. Each system was first energy-minimized for 500 ps, equilibrated at 298 K in the *NVT* ensemble for 100 ps, and then equilibrated at 298 K and 1 atm in the *NPT* ensemble for 100 ps. Simulations were run for 500 ns in explicit water with the TIP3P model[39] at 298 K and 1 atm. A Langevin thermostat was used for temperature control and a Berendsen barostat for pressure control.

We prepared coiled-coil models to append to the two ends of the above set of linker conformers from the published structure of residues 1−30 in the dimer formed by peptide **1** (PDB 4DMD). Coordinates for TOAC in an α-helix[40] were modified to include a virtual atom at the midpoint of the nitroxide N−O bond and incorporated in place of residues 4 and 11 in one chain of the dimer. Residue 14 in the other chain was mutated to Cys, with the side-chain rotamer set as one of the two most probable. Residues near the newly introduced Cys were changed to Ala. All side chains other than those listed above were removed. The above procedure generated two models (A and B), each a dimeric coiled coil doubly labeled with TOAC on one helix. The models differ only in the rotamer of the Cys that will be the point of attachment to the linker.

Capped subunit models were generated using a set of custom-written PyMOL scripts. Coiled-coil models A and B above were first combined with the three different linker conformational ensembles (10,000 frames each) to generate nine sets of capped subunit structures: EDA-A_2, EDA-AB, EDA-B_2, *cis*-PIP-A_2, *cis*-PIP-AB, *cis*-PIP-B_2, *trans*-PIP-A_2, *trans*-PIP-AB, and *trans*-PIP-B_2. Thioethyl groups at each end of the linker were replaced with a coiled coil by overlay of Cys C_α, C_β, and S_γ atoms in the peptide with the corresponding atoms in the linker. The models were combined based on the core linker structure to generate three capped subunit ensembles (EDA, *cis*-PIP, *trans*-PIP). The ensembles were filtered to remove structures with steric clashes, defined as peptide backbone C_α atoms coming within 5 Å of one another or van der Waals overlap[41] involving any pair of atoms.

The resulting ensembles were then filtered further to identify structures consistent with the observed DEER data. A model was accepted only if TOAC−TOAC spin−spin distances for both labeling sites fell within one standard deviation of the most probable distance observed in the DEER experiment. Because the N-terminal labeling site for the PIP linker gave a bimodal distribution in the experiment, capped subunit models based on PIP were divided into two sets (subsets 1 and 2). Conformational ensembles for *cis*-PIP and *trans*-PIP linkers were combined to generate the three conformational ensembles shown in Figure 9 (500−1000 frames were selected at random for each panel): EDA, PIP (subset 1), and PIP (subset 2). The fraction of steric-clash-free models accepted as being consistent with the DEER data by the metrics described above were 43% for EDA, 83% for PIP (subset 1), and 3% for PIP (subset 2).

RESULTS AND DISCUSSION

Design, Synthesis, and Characterization of a Spin-Labeled Homodimeric Coiled Coil. Our first goal was to identify how best to introduce an unpaired electron for ESR

spectroscopy into the dimeric coiled-coil peptide (**1**) that is the basis for the supramolecular polymer assemblies. A widely used method for modifying peptides and proteins with spin labels is the introduction of nitroxide functional groups.[42,43] The nitroxide functionality is most commonly incorporated into expressed proteins via the covalent modification of a cysteine residue with the thiol-reactive reagent MTSSL (termed "site-directed spin labeling").[44−46] In synthetic peptides, nitroxide functionality can also be introduced through incorporation of unnatural monomers, such as the α,α-disubstituted cyclic amino acid TOAC.[47] TOAC offers the advantage over MTSSL of significantly enhanced rigidity. This rigidity enables ESR measurements to report more directly on backbone structure and dynamics than in the case of MTSSL-modified Cys, where side-chain conformational freedom can complicate data interpretation.[48] Drawbacks of TOAC as a spin label include difficult synthesis and the possibility that the unusual topology of the amino acid will disrupt folding. In the context of a coiled coil, the latter issue should not pose a problem due to the high helix propensity of TOAC.[49]

We synthesized and characterized two spin-labeled mutants of peptide **1**, bearing either MTSSL-modified Cys or TOAC (Figure 2). In peptide **2**, a $Ser_{14} \rightarrow$ Cys mutation is made at the

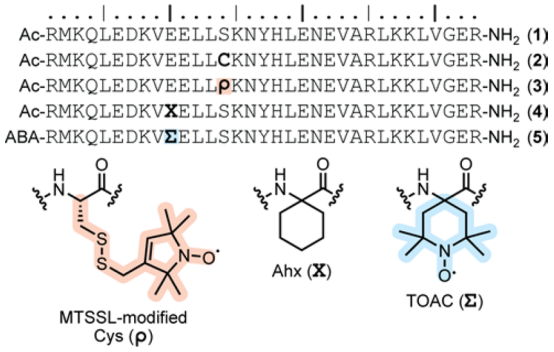

Figure 2. Sequences of peptides **1**−**5** (ABA = 4-acetamidobenzoyl N-terminal cap; Ac = acetyl N-terminal cap) and structures of unnatural amino acid residues MTSSL-Cys, Ahx, and TOAC.

solvent-exposed outer surface of the dimer. Modification of the newly introduced thiol with MTSSL yields MTSSL-Cys-functionalized peptide **3**. On the basis of analysis of the published crystal structure of peptide **1**,[50,51] we identified Glu_{10} as a possible site that would tolerate the steric bulk of a TOAC residue without disrupting the α-helical fold. In order to test this hypothesis, we first examined peptide **4**, in which Glu_{10} is replaced by Ahx, a simplified analogue of TOAC.[49] We grew diffraction-quality crystals of **4** and solved its structure to 1.8 Å resolution. Comparison of the native and mutant crystal structures (Figure 3) shows that the coiled-coil quaternary fold is unperturbed by the cycloalkane backbone modification. Encouraged by the above observations, we synthesized a mutant of **4** with a TOAC in place of Ahx_{10} (peptide **5**).

With two spin-labeled mutants of peptide **1** in hand, we performed DEER measurements to compare MTSSL-modified Cys (peptide **3**) and TOAC (peptide **5**) as probes for elucidating the structure in the coiled-coil quaternary fold. Both labeled peptides gave most probable spin−spin distances in the DEER experiments that were in close agreement with models (Figure 4). Overlay of published coordinates of the MTSSL-modified Cys residue from an α-helix in a small protein[52] on

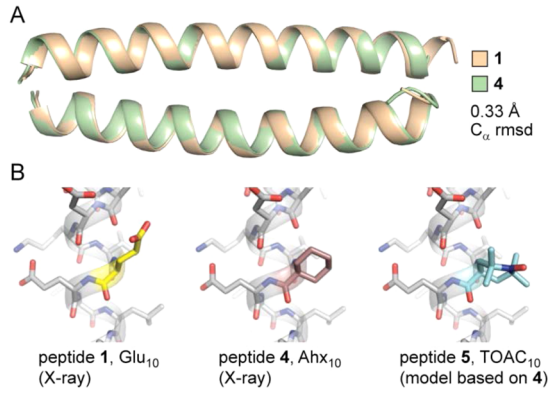

Figure 3. (A) Overlay of the crystal structures of peptide **1** (PDB 4DMD) and peptide **4** (PDB 4TL1). (B) Close-up views of Glu_{10} and Ahx_{10} from the structures of **1** and **4** and a model of the $TOAC_{10}$ residue in **5**.

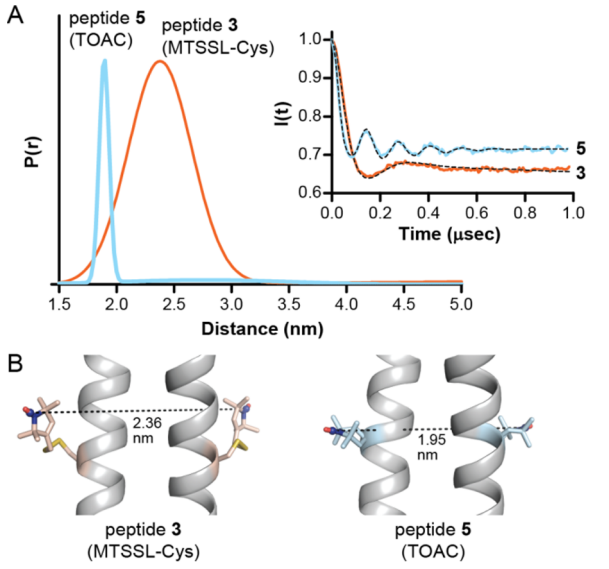

Figure 4. DEER data obtained for peptides **3** and **5**. (A) Background-subtracted time domain signals (inset, solid) fit with Gaussian functions (inset, dashed) and distance distributions resulting from the fit (main graph). Samples were 100 μM peptide in 10 mM HEPES buffer, pH 7 and 20% v/v glycerol. (B) Predicted spin−spin distances for the dimers formed by **3** and **5** based on the structural data for peptides **1** and **4**.

the Ser_{14} residues in the structure of **1** gave a predicted spin−spin distance for the coiled coil formed by peptide **3** (2.36 nm) that was in excellent agreement with experiment (mean of 2.40 nm and standard deviation of 0.26 nm). Similar replacement of the Ahx_{10} residues in the dimer formed by peptide **4** with published coordinates of TOAC in an α-helix context of a small peptide[40] leads to a predicted spin−spin distance for the coiled coil formed by **5** (1.95 nm) that also matches well with experiment (mean of 1.87 nm and standard deviation of 0.07 nm).

Consistent with prior work,[48] the use of TOAC yields a dramatically narrower DEER distance distribution than the conformationally mobile MTSSL spin label. This difference is readily apparent in qualitative comparison of the raw time domain signal for the two peptides (Figure 4A), where at least four full periods are observed for peptide **5** versus only one for peptide **3**. On the basis of the above observations, we selected

dx.doi.org/10.1021/jp505643w | J. Phys. Chem. B 2014, 118, 9881−9889

the TOAC spin label to explore chain dynamics in the coiled-coil supramolecular polymers. The TOAC mutation does not appear to impact the ability of sequence **1** to form its native dimeric fold. Importantly, the standard deviation of the distance distribution is sub-Å, which should ensure that the observed distributions in supramolecular assemblies maximally reflect their conformational preferences.

DEER Analysis of Capped Subunits Based on Homodimeric Coiled-Coil Peptides. The thiol group in Cys-functionalized peptide **2** was reacted with symmetric bis-iodoacetamide linker **6** or **7** to produce subunits **8** and **9** (Figure 5), which are the fundamental building blocks of our

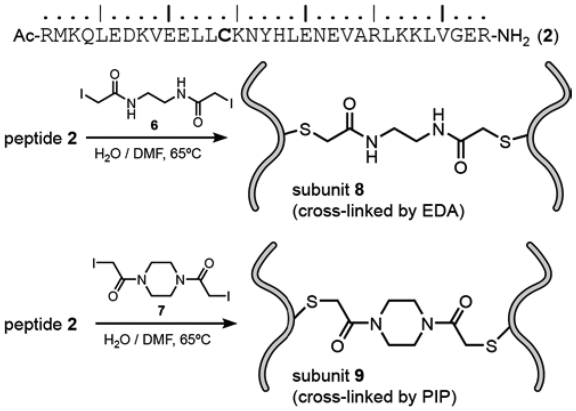

Figure 5. Peptide **2** was used in combination with linker **6** or **7** to prepare cross-linked subunits **8** and **9**.

recently reported coiled-coil supramolecular polymers (Figure 1).[21] We found in prior work that mixing the cross-linked subunit with a non-cross-linked analogue (e.g., peptide **1**) leads the latter to serve as a capping group, adhering to ends of the supramolecular chain.[21] We sought to capitalize on this observation to compare the influence of the two different linkers in **8** and **9** on chain dynamics in the supramolecular polymers that they form upon self-assembly.

We mixed TOAC-labeled peptide **5** with cross-linked subunit **8** or **9** in a ratio intended to give a statistical distribution of products: a homodimeric coiled-coil formed by **5**, a "capped subunit" where two copies of **5** associate with a single cross-linked subunit, and larger oligomers (Figure 6A). On the basis of our prior observations, we anticipated the predominant species in solution would be the capped subunit.[21] The larger oligomers should involve nitroxide−nitroxide distances beyond the range accessible by DEER, and the homodimeric assembly formed by **5** was characterized above. Thus, we hypothesized that any difference that we saw in the ESR data for mixtures of **5** + **8** and **5** + **9** could be attributed to differences in how the organic linkers display the coiled-coil domains.

The DEER data upon mixing spin-labeled probe peptide **5** with cross-linked subunit **8** or **9** are shown in Figure 6B,C. We anticipated a bimodal distribution centered at two distances, a short ∼1.9 nm spin−spin separation corresponding to the homodimer formed by **5** and a longer separation of ∼4−5 nm corresponding to the capped subunit. Initial DEER experiments were carried out with an acquisition time of ∼2.5 μs in an effort to observe both predicted distances; however, a period corresponding to the longer spin−spin separation was not observed in either sample. In order to obtain a more definitive measure of the shorter distance, we repeated the experiments

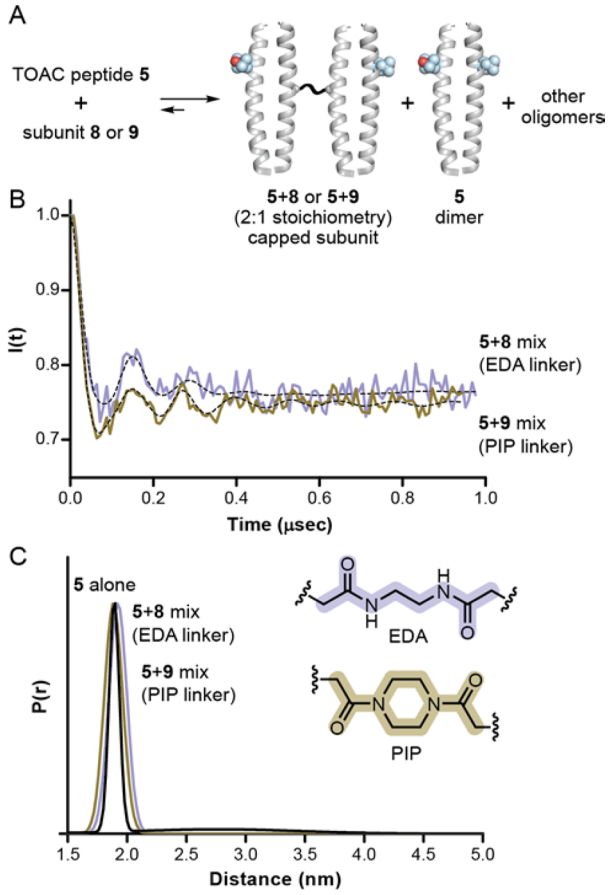

Figure 6. (A) Possible assemblies that can be formed in a mixture of TOAC-labeled peptide **5** with subunit **8** or **9**. (A) Background-subtracted DEER time domain signals (solid) fit with Gaussian functions (dashed) and (B) the distance distributions resulting from the fit. Samples were 100 μM capping peptide **5** and a 33.3 μM subunit (**8** or **9**) in D_2O with 10 mM HEPES buffer, pH 7 and 20% v/v glycerol-d_8.

with a shorter acquisition time (∼1 μs). The result for both samples was a single Gaussian distribution with an average distance of ∼1.9 nm. We interpret this result as suggesting that the equilibrium composition of the mixtures has very little of the desired capped subunit (**5** + **8** or **5** + **9**). Instead, we believe the mixtures favor two other species, the homodimer formed by **5** and longer supramolecular polymers of **8** or **9** capped at their ends by **5**. Strong evidence for the presence of the homodimer of **5** is apparent in the similarity between the observed distance distributions for the binary mixtures and the data for **5** alone (Figure 6C). We infer the presence of longer supramolecular polymers based on the lower signal-to-noise for the binary mixtures compared to that for **5** alone (Figure 6B versus Figure 4A); spins trapped in longer chains would not contribute to the DEER signal due to the very long interspin distances.

The deviation of the equilibrium mixtures away from the desired capped subunit may be a result of an increase in coiled-coil folded stability upon TOAC incorporation. The homodimer formed by **5** showed an unfolding temperature midpoint (T_m) at 71 °C in CD thermal denaturation experiments, compared to 62 °C for wild-type peptide **1** (Figure S1, Supporting Information); we reason that the heterodimer formed by **5** + **1** resides somewhere between these values. This difference in folded stability may be sufficient to skew the

dx.doi.org/10.1021/jp505643w | J. Phys. Chem. B 2014, 118, 9881−9889

expected statistical product distribution that we observed previously when **8** or **9** was mixed with **1**.[21]

Although it may be possible to increase the population of the desired capped subunit by tuning experimental conditions, the above analysis suggested a solution that would be more general, devise a system where the coiled-coil heterodimerization leading to the capped subunit is more favorable than either of the other two possible homodimerization events.

DEER Analysis of Capped Subunits Based on Heterodimeric Coiled-Coil Peptides. We adapted a pair of previously reported heterodimeric coiled-coil sequences from the literature based on peptide **1** for the selective assembly of capped subunits (Figure 7).[53] The peptides **ACID$_{p1}$** and

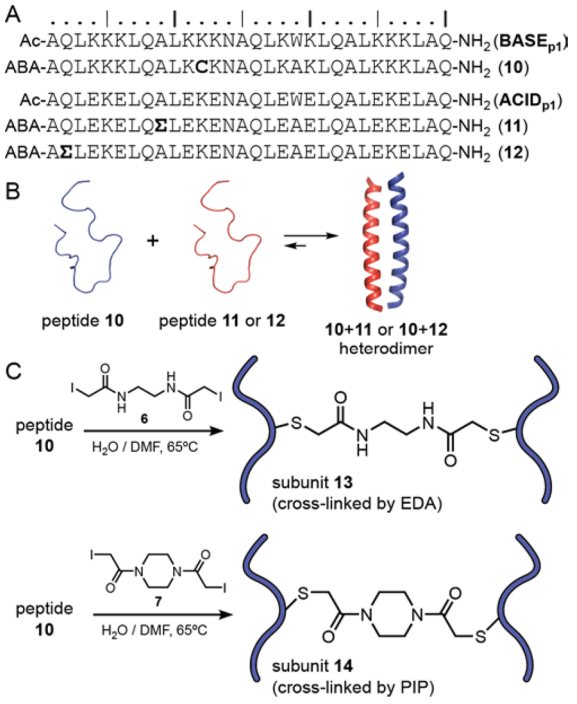

Figure 7. (A) Sequences of peptides **10**−**12** (**Σ** = TOAC; ABA = 4-acetamidobenzoic acid as an N-terminal chromophore cap). (B) Sequences were designed with electrostatic interactions that favor selective formation of heterodimeric assemblies. (C) Peptide **10** was used in combination with linker **6** or **7** to generate cross-linked subunits **13** and **14**.

BASE$_{p1}$ have a similar hydrophobic core composition as sequence **1**, but they differ in residues at the periphery of the interhelical interface of the coiled-coil as well as the solvent-exposed outer surface. In **BASE$_{p1}$**, eight lysine residues are introduced at positions flanking the coiled-coil interface in the folded state to generate a highly cationic sequence. Peptide **ACID$_{p1}$** is identical to **BASE$_{p1}$**, but the lysine residues are replaced with glutamic acids to produce a highly anionic sequence. As a result of the above mutations, homodimerization of either sequence is disfavored by charge repulsion, and the heterodimeric assembly is stabilized by a network of complementary electrostatic interactions.

We prepared three peptides (**10**−**13**) based on the **ACID$_{p1}$**/**BASE$_{p1}$** sequences for use in the selective assembly of a capped subunit for DEER analysis. We introduced a Cys mutation into **BASE$_{p1}$** at a position corresponding to the cross-linking site in peptide **2** to generate peptide **10**. We modified the **ACID$_{p1}$** sequence with TOAC at two different positions to generate peptides **11** and **12**. The other differences between **10**−**13** and the parent **ACID$_{p1}$**/**BASE$_{p1}$** sequences are mutation of Trp_{19} to Ala and the incorporation of 4-acetamidobenzoic acid as a chromophore and N-terminal cap. These alterations were made to facilitate concentration determination and aid in the preparation of mixed samples with accurate stoichiometry. Analysis of the folding behavior of **10**−**13** by CD suggests that, by analogy to the known sequences on which they are based,[53] the **10** + **11** and **10** + **12** heterodimers are more stable than any of the corresponding homodimeric coiled coils (Figure S2, Supporting Information).

We reacted peptide **10** with linker **6** or **7** to produce subunits **13** and **14**. These two subunits were combined with the two different TOAC-functionalized capping peptides **11** and **12** to produce four binary mixtures (Figure 8A). In these four

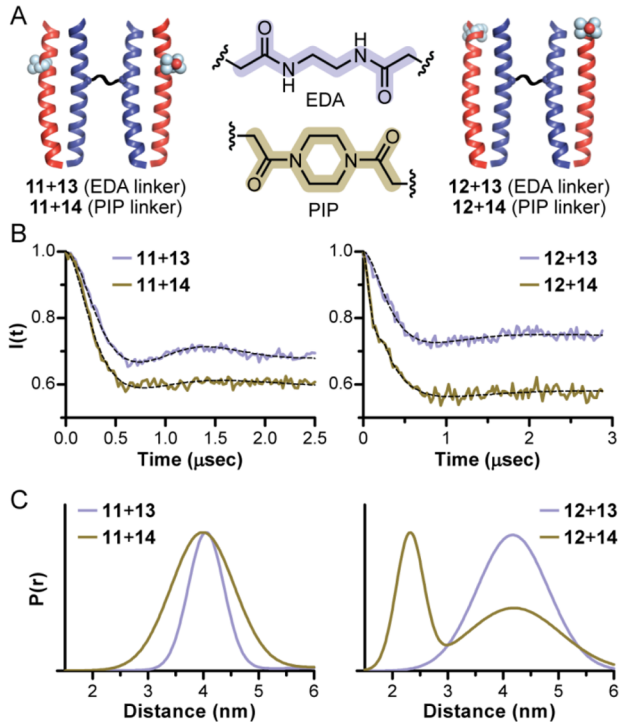

Figure 8. (A) The major species formed upon mixing of capping peptide **11** or **12** with subunit **13** or **14**. (B) Background-subtracted DEER time domain signals (solid) fit with Gaussian functions (dashed) and (C) the distance distributions resulting from the fit. Samples were 100 μM capping peptide (**11** or **12**) and 50 μM subunit (**13** or **14**) in D_2O with 10 mM HEPES buffer, pH 7 and 20% v/v glycerol-d_8.

samples, the identity of the linker and the placement of the nitroxide spin label were systematically varied. On the basis of the preferential heterodimer formation observed upon mixing **10** with **11** or **12**, we reason that the desired capped cross-linked subunit should be the dominant species in solution in each case. The DEER data obtained for the binary mixtures (Figures 8B,C and S3, Supporting Information) were of much higher quality than the statistically controlled homodimer system. Both the placement of the TOAC label and the identity of the linker influenced the distance distribution obtained. With spin-label placement near the cross-linking site (peptide **11** as the capping sequence), the EDA and PIP linkers gave similar most probable distances at ~4.2 nm; however, the more rigid PIP linker gave a wider distribution. When the spin label was

dx.doi.org/10.1021/jp505643w | J. Phys. Chem. B 2014, 118, 9881−9889

placed near the N-terminus (peptide **12** as the capping sequence), the PIP linker exhibited a bimodal distribution with peaks centered at around ∼4.2 and ∼2.3 nm, while the EDA linker showed a single broad distribution at ∼4.2 nm. We chose to use a double Gaussian model to fit the data for **12** + **14** as two modulation periods were observed in the DEER signal; truncation of the data preserves the proportions of the bimodal distribution. The other three samples fit well to a single Gaussian distance distribution. Analysis of the data for **12** + **13** by Tikhanov regularization (Figure S3, Supporting Information) indicated the possibility of a small population with a spin−spin distance of ∼2.3 nm; however, the impact of suppressing this peak on the quality of the fit was small, suggesting a minimal population at most.

MD-Aided Modeling of Capped Subunits. In an effort to gain additional insights into the structure and dynamics in the supramolecular polymers from the ESR data, we carried out MD-aided modeling to identify capped subunit models consistent with the experimental DEER distance distributions. Our approach began with thorough sampling of possible conformations available to each linker alone. We performed separate 500 ns MD simulations on the EDA and PIP linkers with a simple thioethyl moiety attached to the ends. We extracted a random subset of structures from those trajectories and appended coiled coils derived from the known structure of peptide **1** to either end. The resulting ensemble was then filtered to remove frames containing steric clashes involving the newly introduced peptide chains. In a final step, we selected for models in each ensemble that matched the experimental DEER distributions within a standard deviation of the most probable distance for both labeling sites. Because the DEER distribution for the PIP linker and N-terminal labeling site was bimodal, we generated a separate set of structures corresponding to each peak.

Using the above method, we obtained a representative ensemble of ∼1000 models (at ∼4 nm) and ∼500 models (at ∼2.3 nm) for the capped subunits formed by **1** + **8** (EDA linker) and **1** + **9** (PIP linker). It is important to note that while the structures generated sample the conformational space accessible to the supramolecular assemblies based on each linker, they are not true equilibrium distributions. Our approach focused on fine atomistic detail in the linker regions and coarse steric-exclusion effects arising from the two coiled coils being attached in close proximity. We chose the simplified method over more rigorous simulation of the full system due to the computational demands imposed by the latter. The above limitations notwithstanding, there are valuable structural insights to be gained from modeling informed by the ESR experimental data.

In order to visualize dynamics in the supramolecular polymer chain, we focused on the relationship between the backbone C_α atom of Ser_{14} in the two outer helices of the capped subunit (Figure 9A). This position would correspond to the site of cross-linking to the next coiled coil in a larger supramolecular assembly. The most significant difference in the experimental DEER data for capped subunits based on the two linkers was observed when a spin label was incorporated near the N-terminus (Figure 8). The EDA linker showed a unimodal distribution with a most probable spin−spin distance of ∼4 nm, while the PIP linker gave rise to a bimodal distribution with peaks centered at ∼4 and ∼2.3 nm. The capped subunit models for both linkers with a distance between the N-termini of ∼4 nm show a random relative orientation of the two coiled coils

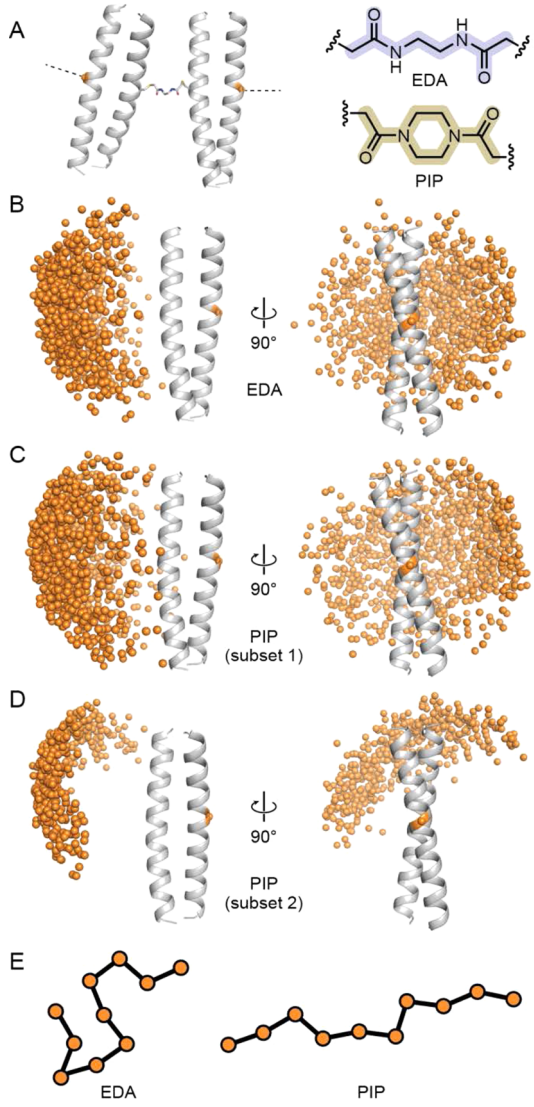

Figure 9. (A) Model of a capped subunit with Ser_{14} residues on the outer helices shown as orange spheres. (B−D) Representative ensemble for a capped subunit with an EDA linker (B) or a PIP linker (C,D). For each panel, models are superimposed based on one of the two coiled coils (cartoon), and the position of the second coiled coil is indicated by a single orange sphere, the point of attachment to the next link in the supramolecular polymer chain. (E) Simplified schematic showing different chain stiffness in the supramolecular polymers based on the EDA versus PIP linker.

and a wide distribution of possible ways that the supramolecular polymer chain can progress at the junction. By contrast, the shorter ∼2.3 nm distance between N-termini observed for the PIP linker corresponds to a set of structures where the two coiled coils are oriented roughly parallel and the positioning of cross-linking sites on the outer helices is severely restricted.

We hypothesize that the subpopulation of PIP-linked coiled coils with restricted motions along the chain would propagate the polymer in approximately the same direction at each such subunit, thereby increasing the chain stiffness and persistence length (Figure 9E). For the EDA linker, the relative positioning of cross-linking sites is more randomly distributed, giving rise to a supramolecular chain capable of forming more compact structures with shorter persistence length. The above analysis

dx.doi.org/10.1021/jp505643w | J. Phys. Chem. B 2014, 118, 9881−9889

provides direct structural explanation as to how small differences in linker rigidity in cross-linked subunits **8** and **9** can propagate along the supramolecular polymer chain.

CONCLUSIONS

In summary, we have reported here the application of DEER spectroscopy to probe the structure and chain flexibility in supramolecular polymers based on coiled-coil-forming peptide domains bridged by small organic linkers. Our results provide insights into how subtle changes to linker flexibility can influence the relationship between adjacent coiled coils in the supramolecular polymer chain. The key experimental considerations necessary to obtain high-quality ESR data bearing on these questions was the use of the rigid nitroxide spin label TOAC in a system of peptides that is capable of highly selective self-assembly to form a capped subunit with minimal contamination by other species in solution.

Our results reveal that a linker with fewer rotational degrees of freedom appears to stabilize a folded population of cross-linked coiled coils with N-termini of adjacent dimers in close proximity. MD simulations, guided by the experimental DEER data, suggest a structural picture as to how this population of conformers stiffens the supramolecular polymer chain, giving rise to a larger apparent hydrodynamic diameter without an accompanying increase in chain length. Our findings show how very small changes in covalent structure of a self-assembling subunit (addition of two CH_2 groups to an 8 kDa monomer) can have a pronounced effect on the physical properties of a chain formed upon supramolecular polymerization of that subunit. Moreover, these results highlight the value of DEER spectroscopy for elucidating complex dynamics in designed protein-based materials.

ASSOCIATED CONTENT

Supporting Information

Coordinates and structure factors for peptide **4** have been deposited in the PDB under accession code 4TL1. Figures S1–S9 and Tables S1 and S2 are also available, showing extinction coefficients of the peptides and cross-linked subunits, X-ray diffraction data, circular dichroism thermal melts, circular dichroism spectra, background-subtracted DEER time domain signals, distance distributions, comparisons between DEER data, and raw DEER data. This material is available free of charge via the Internet at http://pubs.acs.org.

AUTHOR INFORMATION

Corresponding Authors

*E-mail: sksaxena@pitt.edu (S.S.).
*E-mail: horne@pitt.edu (W.S.H.).

Author Contributions

†N.A.T. and K.I.S. contributed equally.

Notes

The authors declare no competing financial interest.

ACKNOWLEDGMENTS

Funding for this work was provided by the University of Pittsburgh and the National Science Foundation (MCB1157712 to S.S., CAREER award DMR1149067 to W.S.H.). The Bruker ElexSys E680 was purchased with funds from National Institutes of Health Grant 1S10RR028701. This research was supported in part by the University of Pittsburgh Center for Simulation and Modeling through the supercomputing resources provided. We specifically acknowledge the assistance of Albert DeFusco in the use of these computational resources.

REFERENCES

(1) Brunsveld, L.; Folmer, B. J. B.; Meijer, E. W.; Sijbesma, R. P. Supramolecular Polymers. *Chem. Rev.* **2001**, *101*, 4071–4098.
(2) Lehn, J.-M. Supramolecular Polymer Chemistry—Scope and Perspectives. *Polym. Int.* **2002**, *51*, 825–839.
(3) Yan, Y.; Lin, Y.; Qiao, Y.; Huang, J. Construction and Application of Tunable One-Dimensional Soft Supramolecular Assemblies. *Soft Matter* **2011**, *7*, 6385–6398.
(4) Aida, T.; Meijer, E. W.; Stupp, S. I. Functional Supramolecular Polymers. *Science* **2012**, *335*, 813–817.
(5) Lehn, J.-M. Dynamers: Dynamic Molecular and Supramolecular Polymers. *Prog. Polym. Sci.* **2005**, *30*, 814–831.
(6) Hirst, A. R.; Escuder, B.; Miravet, J. F.; Smith, D. K. High-Tech Applications of Self-Assembling Supramolecular Nanostructured Gel-Phase Materials: From Regenerative Medicine to Electronic Devices. *Angew. Chem., Int. Ed.* **2008**, *47*, 8002–8018.
(7) Krieg, E.; Rybtchinski, B. Noncovalent Water-Based Materials: Robust yet Adaptive. *Chem.—Eur. J.* **2011**, *17*, 9016–9026.
(8) Rybtchinski, B. Adaptive Supramolecular Nanomaterials Based on Strong Noncovalent Interactions. *ACS Nano* **2011**, *5*, 6791–6818.
(9) Boyle, A. L.; Woolfson, D. N. Rational Design of Peptide-Based Biosupramolecular Systems. In *Supramolecular Chemistry: From Molecules to Nanomaterials*; Gale, P. A., Steed, J. W., Eds.; John Wiley and Sons: New York, 2012; Vol. *8*, pp 1639–1664.
(10) Doles, T.; Bozic, S.; Gradisar, H.; Jerala, R. Functional Self-Assembling Polypeptide Bionanomaterials. *Biochem. Soc. Trans.* **2012**, *40*, 629–634.
(11) Crick, F. The Packing of α-Helices: Simple Coiled-Coils. *Acta Crystallogr.* **1953**, *6*, 689–697.
(12) Lupas, A. N.; Gruber, M. The Structure of α-Helical Coiled Coils. *Adv. Protein Chem.* **2005**, *70*, 37–78.
(13) Parry, D. A.; Fraser, R. D.; Squire, J. M. Fifty Years of Coiled-Coils and α-Helical Bundles: A Close Relationship between Sequence and Structure. *J. Struct. Biol.* **2008**, *163*, 258–269.
(14) Ciani, B.; Bjelic, S.; Honnappa, S.; Jawhari, H.; Jaussi, R.; Payapilly, A.; Jowitt, T.; Steinmetz, M. O.; Kammerer, R. A. Molecular Basis of Coiled-Coil Oligomerization-State Specificity. *Proc. Natl. Acad. Sci. U.S.A.* **2010**, *107*, 19850–19855.
(15) Reinke, A. W.; Grant, R. A.; Keating, A. E. A Synthetic Coiled-Coil Interactome Provides Heterospecific Modules for Molecular Engineering. *J. Am. Chem. Soc.* **2010**, *132*, 6025–6031.
(16) Grigoryan, G.; Degrado, W. F. Probing Designability via a Generalized Model of Helical Bundle Geometry. *J. Mol. Biol.* **2011**, *405*, 1079–1100.
(17) Xu, C.; et al. Rational Design of Helical Nanotubes from Self-Assembly of Coiled-Coil Lock Washers. *J. Am. Chem. Soc.* **2013**, *135*, 15565–15578.
(18) Ryadnov, M. G. A Self-Assembling Peptide Polynanoreactor. *Angew. Chem., Int. Ed.* **2007**, *46*, 969–972.
(19) Fletcher, J. M.; et al. Self-Assembling Cages from Coiled-Coil Peptide Modules. *Science* **2013**, *340*, 595–599.
(20) Zhou, M.; Bentley, D.; Ghosh, I. Helical Supramolecules and Fibers Utilizing Leucine Zipper-Displaying Dendrimers. *J. Am. Chem. Soc.* **2004**, *126*, 734–735.
(21) Staples, J. K.; Oshaben, K. M.; Horne, W. S. A Modular Synthetic Platform for the Construction of Protein-Based Supramolecular Polymers via Coiled-Coil Self-Assembly. *Chem. Sci.* **2012**, *3*, 3387–3392.
(22) Oshaben, K. M.; Horne, W. S. Tuning Assembly Size in Peptide-Based Supramolecular Polymers by Modulation of Subunit Association Affinity. *Biomacromolecules* **2014**, *15*, 1436–1442.
(23) Milov, A. D.; Ponomarev, A. B.; Tsvetkov, Y. D. Electron–Electron Double Resonance in Electron Spin Echo: Model Biradical

Systems and the Sensitized Photolysis of Decalin. *Chem. Phys. Lett.* **1984**, *110*, 67−72.
(24) Pannier, M.; Veit, S.; Godt, A.; Jeschke, G.; Spiess, H. W. Dead-Time Free Measurement of Dipole−Dipole Interactions between Electron Spins. *J. Magn. Reson.* **2000**, *142*, 331−340.
(25) Jeschke, G. DEER Distance Measurements on Proteins. *Annu. Rev. Phys. Chem.* **2012**, *63*, 419−446.
(26) Bowman, A.; Hammond, C. M.; Stirling, A.; Ward, R.; Shang, W.; El-Mkami, H.; Robinson, D. A.; Svergun, D. I.; Norman, D. G.; Owen-Hughes, T. The Histone Chaperones Vps75 and Nap1 Form Ring-Like, Tetrameric Structures in Solution. *Nucleic Acids Res.* **2014**, *42*, 6038−6051.
(27) Coin, I.; Beyermann, M.; Bienert, M. Solid-Phase Peptide Synthesis: From Standard Procedures to the Synthesis of Difficult Sequences. *Nat. Protoc.* **2007**, *2*, 3247−3256.
(28) Kaduk, C.; Wenschuh, H.; Beyermann, M.; Forner, K.; Carpino, L.; Bienert, M. Synthesis of Fmoc-Amino Acid Fluorides via DAST, an Alternative Fluorinating Agent. *Lett. Pept. Sci.* **1995**, *2*, 285−288.
(29) Martin, L.; Ivancich, A.; Vita, C.; Formaggio, F.; Toniolo, C. Solid-Phase Synthesis of Peptides Containing the Spin-Labeled 2,2,6,6-Tetramethylpiperidine-1-oxyl-4-amino-4-carboxylic Acid (TOAC). *J. Pept. Res.* **2001**, *58*, 424−432.
(30) Karim, C. B.; Zhang, Z.; Thomas, D. D. Synthesis of TOAC Spin-Labeled Proteins and Reconstitution in Lipid Membranes. *Nat. Protoc.* **2007**, *2*, 42−49.
(31) Adams, P. D.; et al. PHENIX: A Comprehensive Python-Based System for Macromolecular Structure Solution. *Acta Crystallogr., Sect D* **2010**, *66*, 213−221.
(32) Emsley, P.; Lohkamp, B.; Scott, W. G.; Cowtan, K. Features and Development of Coot. *Acta Crystallogr., Sect D* **2010**, *66*, 486−501.
(33) Martin, R. E.; Pannier, M.; Diederich, F.; Gramlich, V.; Hubrich, M.; Spiess, H. W. Determination of End-to-End Distances in a Series of TEMPO Diradicals of up to 2.8 nm Length with a New Four-Pulse Double Electron Electron Resonance Experiment. *Angew. Chem., Int. Ed.* **1998**, *37*, 2833−2837.
(34) Jeschke, G.; Chechik, V.; Ionita, P.; Godt, A.; Zimmermann, H.; Banham, J.; Timmel, C. R.; Hilger, D.; Jung, H. DeerAnalysis2006: A Comprehensive Software Package for Analyzing Pulsed ELDOR Data. *Appl. Magn. Reson.* **2006**, *30*, 473−498.
(35) Pronk, S.; et al. GROMACS 4.5: A High-Throughput and Highly Parallel Open Source Molecular Simulation Toolkit. *Bioinformatics* **2013**, *29*, 845−854.
(36) Lindorff-Larsen, K.; Piana, S.; Palmo, K.; Maragakis, P.; Klepeis, J. L.; Dror, R. O.; Shaw, D. E. Improved Side-Chain Torsion Potentials for the Amber ff99sb Protein Force Field. *Proteins: Struct., Funct., Bioinf.* **2010**, *78*, 1950−1958.
(37) Wang, J.; Wang, W.; Kollman, P. A.; Case, D. A. Automatic Atom Type and Bond Type Perception in Molecular Mechanical Calculations. *J. Mol. Graphics Modell.* **2006**, *25*, 247−260.
(38) Sousa da Silva, A.; Vranken, W. ACPYPE — Antechamber Python Parser Interface. *BMC Res. Notes* **2012**, *5*, 367.
(39) Jorgensen, W. L.; Chandrasekhar, J.; Madura, J. D.; Impey, R. W.; Klein, M. L. Comparison of Simple Potential Functions for Simulating Liquid Water. *J. Chem. Phys.* **1983**, *79*, 926−935.
(40) Saviano, M.; Improta, R.; Benedetti, E.; Carrozzini, B.; Cascarano, G. L.; Didierjean, C.; Toniolo, C.; Crisma, M. Benzophenone Photophore Flexibility and Proximity: Molecular and Crystal-State Structure of a Bpa-Containing Trichogin Dodecapeptide Analogue. *ChemBioChem* **2004**, *5*, 541−544.
(41) Seeliger, D.; de Groot, B. L. Atomic Contacts in Protein Structures. A Detailed Analysis of Atomic Radii, Packing, and Overlaps. *Proteins: Struct., Funct., Bioinf.* **2007**, *68*, 595−601.
(42) Stone, T. J.; Buckman, T.; Nordio, P. L.; McConnell, H. M. Spin-Labeled Biomolecules. *Proc. Natl. Acad. Sci. U.S.A.* **1965**, *54*, 1010−1017.
(43) Keana, J. F. W. Newer Aspects of the Synthesis and Chemistry of Nitroxide Spin Labels. *Chem. Rev.* **1978**, *78*, 37−64.
(44) Altenbach, C.; Flitsch, S. L.; Khorana, H. G.; Hubbell, W. L. Structural Studies on Transmembrane Proteins. 2. Spin Labeling of Bacteriorhodopsin Mutants at Unique Cysteines. *Biochemistry* **1989**, *28*, 7806−7812.
(45) Altenbach, C.; Marti, T.; Khorana, H.; Hubbell, W. Transmembrane Protein Structure: Spin Labeling of Bacteriorhodopsin Mutants. *Science* **1990**, *248*, 1088−1092.
(46) Columbus, L.; Hubbell, W. L. A New Spin on Protein Dynamics. *Trends Biochem. Sci.* **2002**, *27*, 288−295.
(47) Schreier, S.; Bozelli, J.; Marín, N.; Vieira, R.; Nakaie, C. The Spin Label Amino Acid TOAC and Its Uses in Studies of Peptides: Chemical, Physicochemical, Spectroscopic, and Conformational Aspects. *Biophys. Rev.* **2012**, *4*, 45−66.
(48) Smythe, M. L.; Nakaie, C. R.; Marshall, G. R. α-Helical Versus 3_{10}-Helical Conformation of Alanine-Based Peptides in Aqueous Solution: An Electron Spin Resonance Investigation. *J. Am. Chem. Soc.* **1995**, *117*, 10555−10562.
(49) Toniolo, C.; et al. Synthesis and Conformational Studies of Peptides Containing TOAC, a Spin-Labelled $C^{\alpha,\alpha}$-Disubstituted Glycine. *J. Pept. Sci.* **1995**, *1*, 45−57.
(50) O'Shea, E. K.; Klemm, J. D.; Kim, P. S.; Alber, T. X-Ray Structure of the GCN4 Leucine Zipper, a Two-Stranded, Parallel Coiled Coil. *Science* **1991**, *254*, 539−544.
(51) Oshaben, K. M.; Salari, R.; McCaslin, D. R.; Chong, L. T.; Horne, W. S. The Native GCN4 Leucine-Zipper Domain Does Not Uniquely Specify a Dimeric Oligomerization State. *Biochemistry* **2012**, *51*, 9581−9591.
(52) Cunningham, T. F.; McGoff, M. S.; Sengupta, I.; Jaroniec, C. P.; Horne, W. S.; Saxena, S. High-Resolution Structure of a Protein Spin-Label in a Solvent-Exposed β-Sheet and Comparison with DEER Spectroscopy. *Biochemistry* **2012**, *51*, 6350−6359.
(53) O'Shea, E. K.; Lumb, K. J.; Kim, P. S. Peptide 'Velcro': Design of a Heterodimeric Coiled Coil. *Curr. Biol.* **1993**, *3*, 658−667.